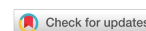


Research Article

Open Access



Citric acid-based degradable polyester elastomers coated with silver nanowires for sustainable soft sensors

Zhao Wang, Hongwei Zhou*, Bohui Zheng, Yang Gao, Hongli Zhang, Xilang Jin, Gai Zhang, Aijie Ma

Shaanxi Key Laboratory of Photoelectric Functional Materials and Devices, School of Materials and Chemical Engineering, Xi'an Technological University, Xi'an 710021, Shaanxi, China.

* **Correspondence to:** Prof. Hongwei Zhou, Shaanxi Key Laboratory of Photoelectric Functional Materials and Devices, School of Materials and Chemical Engineering, Xi'an Technological University, No. 2 Middle Xuefu Road, Weiyang District, Xi'an 710021, Shaanxi, China. E-mail: xatuzhou@163.com or xatuzhou@xatu.edu.cn

How to cite this article: Wang Z, Zhou H, Zheng B, Gao Y, Zhang H, Jin X, Zhang G, Ma A. Citric acid-based degradable polyester elastomers coated with silver nanowires for sustainable soft sensors. *Soft Sci* 2022;2:16. <https://dx.doi.org/10.20517/ss.2022.14>

Received: 6 Jul 2022 **First Decision:** 28 Jul 2022 **Revised:** 27 Aug 2022 **Accepted:** 13 Sep 2022 **Published:** 22 Sep 2022

Academic Editor: Zhifeng Ren **Copy Editor:** Fangling Lan **Production Editor:** Fangling Lan

Abstract

Although soft electronic materials are of significant importance for flexible electronic devices, most of them are derived from commercial polymer elastomers, such as polydimethylsiloxane, polyurethane and Ecoflex. In this work, citric acid-based degradable polyester elastomers are prepared by a melt polycondensation process, utilizing citric acid, 1,8-octanediol and poly(ethylene glycol) (PEG) as monomers. Furthermore, poly(1,8-octanediol citrate acid) (POC)-PEG/silver nanowire (AgNW) conductive polyester elastomers (CPEs) are prepared by introducing a AgNW layer on the surface of the POC-PEG films. Scanning electron microscopy images reveal that the thickness of the AgNW layer is on the scale of several micrometers and the AgNWs form a continuous conductive network. Upon mechanical stimuli, POC-PEG exhibits recoverable deformation and induces variation in the AgNW conductive network, resulting in a conversion of strain to detectable resistance. When tensile strain is applied, the POC-PEG/AgNW CPEs achieve a gauge factor of 231.6, a response range of 0%-50%, a low response time of 35 ms and high stability. Moreover, the POC-10PEG/AgNW CPE also responds to bending deformation with a gauge factor of 3667.5, a response range of 0%-8.4%, a low response time of 62 ms and high stability. On the basis of strain sensitivity, wireless sensors are further assembled by integrating the POC-PEG/AgNW CPEs into a Bluetooth signal transmission system. Various human motions and physiological activities are successfully monitored using the wireless sensors. The results demonstrate that degradable citric acid-based polyester elastomers/AgNW CPEs are promising materials for next-generation sustainable and flexible electronic devices.



© The Author(s) 2022. **Open Access** This article is licensed under a Creative Commons Attribution 4.0 International License (<https://creativecommons.org/licenses/by/4.0/>), which permits unrestricted use, sharing, adaptation, distribution and reproduction in any medium or format, for any purpose, even commercially, as long as you give appropriate credit to the original author(s) and the source, provide a link to the Creative Commons license, and indicate if changes were made.



Keywords: Polyester elastomers, citric acid, AgNWs, strain sensitivity, degradable

INTRODUCTION

Soft electronic materials are of great significance for flexible electronic devices^[1-6]; however, most of them are nanocomposites of commercial elastomers and conductive fillers. Commercial elastomers include polydimethylsiloxane (PDMS)^[7-11], polyurethane (PU)^[12,13] and Ecoflex^[14,15], and conductive nanomaterials, such as metal and carbon nanomaterials, MXenes and liquid metals^[16-21], are mainly utilized as conductive fillers. In such nanocomposites, the properties of commercial elastomers are difficult to control due to their fixed structures. Moreover, most elastomers have poor degradability and biocompatibility, which limits their applications in sustainable and bio-related electronic devices^[22,23]. The development of high-performance soft electronic materials for next-generation sustainable and wearable devices is therefore a crucial research area.

Polyester elastomers represent a class of polymers containing abundant ester groups in polymer chains and possess a glass transition temperature (T_g) lower than room temperature. By tuning their structure, polyester elastomers can achieve comparable mechanical properties to that of most commercial elastomers, including strength, elongation at break and resilience. In particular, polyester elastomers have obvious advantages over other polymer elastomers (e.g., PDMS and PU) regarding degradability and biocompatibility, thereby making polyester elastomers soft and environmentally-friendly polymer materials^[24-29]. Significant attention has been devoted to developing new polyester elastomers with high mechanical properties. For instance, polyester elastomers prepared from bis(β -lactone) and star-shaped hydroxyl-terminated poly(γ -methyl- ϵ -caprolactone) achieved a high breaking stress of 6 MPa, a Young's modulus of 2 MPa and an elongation at break of 850%. Moreover, such polyester elastomers have the ability to degrade within 60 h at pH 7 and 40 °C^[30]. Interestingly, Zhang and co-workers systematically investigated a series of polyester elastomers utilizing bio-monomers or bio-derived monomers. The tensile strength and elongation at break can be controlled in the ranges of 1.2-16.0 MPa and 70%-800%, respectively, and such polyester elastomers also show excellent biocompatibility and promising applications in in-vivo soft tissue repair^[31-34]. However, there has still been less work on the use of polyester elastomers in soft electronics.

Citric acid is a low-cost organic acid that widely exists in fruits (such as lemon, citrus, pineapple and others) and animals (bones, muscles and blood). In addition, citric acid can also be synthesized by a fermentation procedure utilizing sugar-containing raw materials. Citric acid is non-toxic and has been extensively used as a food additive. From the perspective of chemical structure, one citric acid molecule contains three carboxyl groups and one hydroxyl group, which can react with other monomers containing hydroxyl, carboxyl and amino groups by a condensation process. Citric acid is an important monomer in the preparation of degradable polyester elastomers. The development of citric acid-based degradable polyester elastomers may provide new insights for the fabrication of sustainable and flexible soft electronic devices.

Herein, degradable citric acid-based conductive polyester elastomer (CPEs) are developed and used in constructing soft and wearable sensors. The degradable polyester elastomers are prepared by a melt polycondensation utilizing citric acid (CA), 1,8-octanediol and poly(ethylene glycol) (PEG) as monomers. Condensation polymerization of CA and 1,8-octanediol leads to the formation of poly(1,8-octanediol citrate) (POC). PEG is used as a flexible monomer to tune the mechanical properties. Silver nanowires (AgNW) is introduced on the surface of the POC-PEG films to make CA-based polyester elastomer/AgNW CPEs. The strain sensitivity of the POC-PEG/AgNW CPEs is investigated, and soft and wearable sensors are fabricated on their basis.

EXPERIMENTAL

Materials

CA ($\geq 99.5\%$) was purchased from the Tianjin Damao Chemical Reagent Factory. 1,8-octanediol (98%), PEG ($M_n = 2000$) and phosphate-buffered saline (PBS) (pH 7.3) were supplied by Shanghai Aladdin Bio-Chem Technology Co., Ltd. AgNW was prepared according to a previously reported method^[35].

Preparation of degradable POC-PEG polyester elastomers

The POC-PEG elastomers were synthesized by a melt polycondensation method and the detailed procedures were as follows. Under nitrogen protection and magnetic stirring, CA and 1,8-octanediol (molar ratio of 1.1:1) were added to a three-necked flask and heated to 140 °C to obtain a melt. PEG with different mass fractions was then added to the above melt and stirred to form a homogeneous solution. The polymerization was conducted at 140 °C for 0.5 h to obtain a viscous prepolymer mixture that was poured into a Teflon mold. The polymerization was further conducted at 80 °C for 72 h to obtain the target POC-PEG elastomers. By adjusting the mass fraction of PEG (0, 10 and 20 wt.%), different polyester elastomers (POC, POC-10PEG and POC-20PEG) were obtained.

Preparation of POC-PEG/AgNW CPEs

POC-PEG/AgNW CPEs were prepared as follows. A AgNW dispersion in ethanol (1 mg mL^{-1}) was prepared with the assistance of ultrasound and then introduced onto the surface of the POC-PEG films by a droplet coating procedure. The thickness of the AgNW layer was controlled by the coating time.

Fabrication of flexible strain sensors using POC-PEG/AgNW CPEs

Flexible strain sensors were fabricated as follows. The POC-10PEG CPE was tailored into dimensions of $45 \text{ mm} \times 10 \text{ mm} \times 2 \text{ mm}$. Two wires were then connected to the ends of the POC-PEG/AgNW CPE to obtain flexible strain sensors. Wireless sensors were fabricated by connecting the flexible strain sensors to a Bluetooth signal transmission system, as described in our previous work^[36,37].

Characterization

Fourier transform infrared (FT-IR) spectra were collected on a Nicolet IS50 FT-IR spectrometer. The samples were coated on potassium bromide salt sheets and the scanning range was $400\text{-}4000 \text{ cm}^{-1}$.

The ultraviolet-visible (UV-Vis) spectra of the AgNW were collected on a Shimadzu UV-2550. AgNW was dispersed in ethanol and the concentration was 0.01 mg mL^{-1} . The scanning range was 200-800 nm. The surface and fracture morphology of the AgNW and POC-PEG/AgNW CPEs were observed using scanning electron microscopy (SEM, VEGA II XMU). The samples were sputtered with gold in a vacuum prior to observation.

Thermogravimetric analysis (TGA) was performed on a thermogravimetric analyzer (METTLER TOLEDO TGA/DSC) with a nitrogen flow of 50 mL min^{-1} . The weight loss of the sample was recorded by heating the sample from 25 to 600 °C at a heating rate of 10 °C min^{-1} .

The glass transition temperature (T_g) was obtained from differential scanning calorimetry (DSC) curves of the polyester elastomers. The DSC curves were collected on a differential scanning calorimeter (METTLER TOLEDO DSC823e) under a N_2 atmosphere. The heating rate was 10 °C min^{-1} and the scanning range was -50-150 °C.

The stress-strain curves and tensile load-unload curves of the polyester elastomers were recorded on a universal testing machine (CMT2500). The sample size was 75 mm × 4 mm × 2 mm and the stretching speed was 20 mm min⁻¹. The elastic modulus (E) of the POC-PEG elastomers was obtained from the slope of the stress-strain curve in the strain range of 0%-25% according to $E = \Delta\sigma/\Delta\varepsilon$, in which σ and ε are stress and strain, respectively.

For the degradability test, a piece of POC-PEG/AgNW CPE was immersed in a PBS solution or 0.1 mol L⁻¹ NaOH aqueous solution at room temperature. Morphological changes were recorded by taking photographs at different time intervals. The gel permeation chromatography curves of the polyester elastomer prepolymer and POC-PEG/AgNW CPEs after being degraded in a 0.1 mol L⁻¹ NaOH aqueous solution for 10 d were collected to evaluate the degradability.

The strain sensitivity, sensing stability, response time and resistive response to different strains were evaluated by recording the resistance change of the POC-PEG/AgNW CPEs under different applied strains. The sensors were fixed on a homemade electromotor reciprocating device and the strain was applied in different modes. During cyclic deformation, the resistance change was recorded by a digital bridge (LCR, UC2858A) [Supplementary Figure 1] equipped with a computer. The relative resistance change ($\Delta R/R_0$) was calculated according to $\Delta R/R_0 = (R_i - R_0)/R_0$, where R_0 and R_i represent the initial resistance of the POC-PEG/AgNW CPE and resistance under an applied strain, respectively.

RESULTS AND DISCUSSION

Preparation and properties of POC-PEG/AgNW CPEs

The degradable POC-PEG polyester elastomers were prepared according to the synthetic route shown in Figure 1A. The POC-PEG elastomers were prepared based on a polycondensation process. CA was selected as the carboxyl group-containing monomer. Because the CA molecule has three carboxyl groups and one hydroxyl group, it also works as a crosslinker to bond polyester chains together. The preparation of the POC-PEG elastomers was conducted via a two-stage process of prepolymerization and post-polymerization and the feeding ratio of PEG was adjusted to prepare POC-PEG elastomers with different chemical structures. Figure 1B shows the FT-IR spectra of the monomers and POC-PEG elastomers. For POC, POC-10PEG and POC-20PEG, the characteristic peaks at 1732 and 1193 cm⁻¹ are related to the stretching vibration of the C=O and C-O bonds in the ester groups, respectively. Compared with the POC elastomer, the POC-PEG elastomer showed a new absorption peak at 950 cm⁻¹, which was the symmetric stretching vibration peak of the ether bond (C-O-C), indicating the successful preparation of POC-PEG elastomers [Figure 1C].

The glass transition temperature (T_g) of the POC-PEG elastomers was obtained from the DSC curves. As shown in Figure 2A, all the samples, including POC, POC-10PEG and POC-20PEG, exhibit an obvious glass transition. Because the T_g values are all below room temperature, POC, POC-10PEG and POC-20PEG are in their highly elastic state. With an increase in PEG content from 0 to 20 wt.%, T_g decreases from 1.3 to -17.4 °C, indicating that PEG works as a soft segment in POC-PEG elastomers. In addition, PEG has a relatively long molecular chain compared with other small monomers. The crosslinking density of elastomers is lowered when the PEG content is increased, which also helps to promote the chain segment motion of polymers and leads to decreased T_g .

Figure 2B shows the TG curves of POC, POC-10PEG and POC-20PEG. As seen, POC, POC-10PEG and POC-20PEG show good thermal stability below 210 °C. Between 210 and 500 °C the elastomers exhibit an obvious weight loss. There are two weight loss stages at 210-300 and 300-550 °C, respectively. At

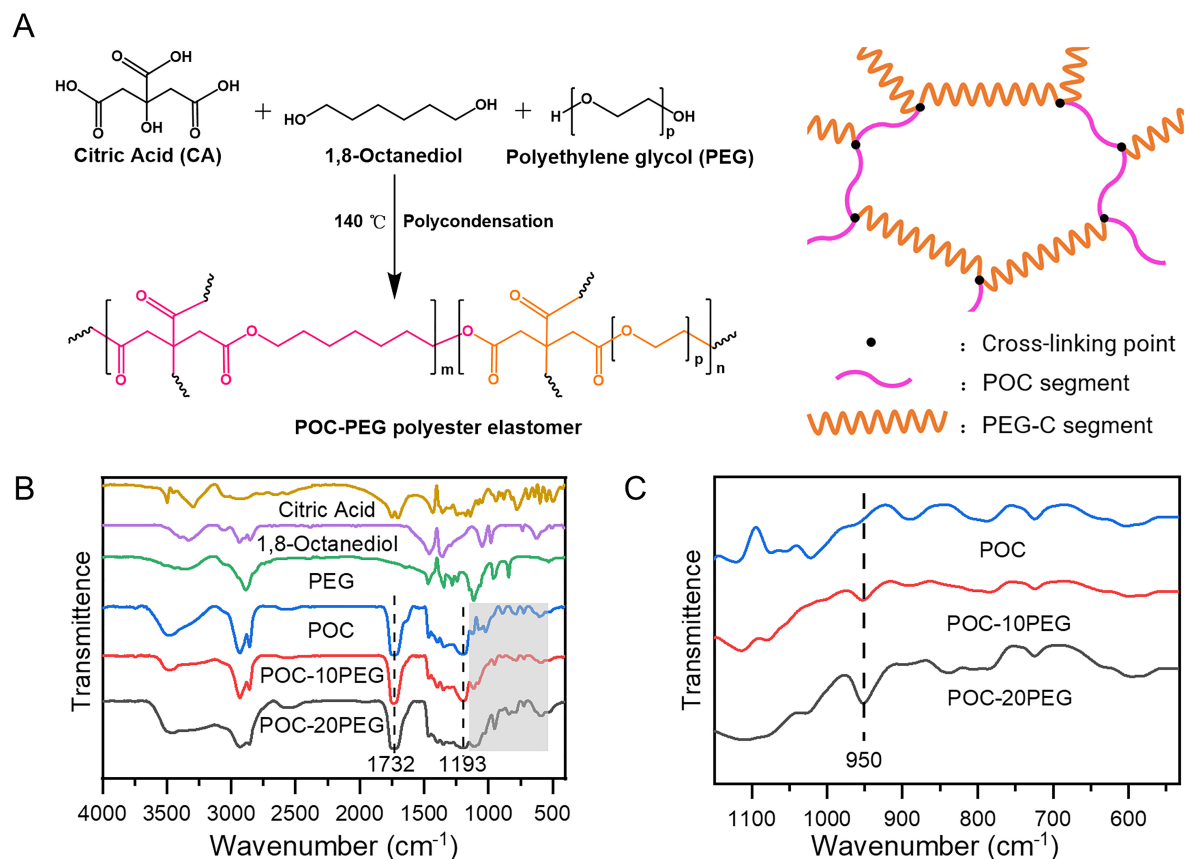


Figure 1. (A) Synthetic route for POC-PEG degradable polyester elastomers. (B) FT-IR spectra of monomers and POC-PEG elastomers with different PEG contents. (C) Enlarged infrared spectra of highlighted section in (B).

210–300 °C, the weight loss is ~20% and the weight loss rate is relatively low, while at 300–550 °C, the weight loss is ~70% and the weight loss rate is relatively high. The first weight loss stage may be related to the separation of small molecules from the polymer network. In the second stage, the ester bonds and carbon-carbon bonds existing in the polymer network are broken and the polymer network disintegrates into segments, thereby inducing a rapid weight loss.

Because of the low T_g , the POC-PEG elastomers exhibit excellent elasticity and stretchability. POC, POC-10PEG and POC-20PEG are all stretchable with an elongation at break of > 50% [Figure 2C]. With increasing PEG content, the breaking strength and Young's modulus of the elastomers decreased, while the elongation at break obviously increased. For POC-10PEG, the breaking strength and the elongation at break are 0.6 MPa and 160%, respectively. Figure 2D shows that Young's modulus decreases from 2.39 to 0.16 MPa and the elongation at break increases from 67.2% to 254.7% when the PEG content increases from 0 to 20 wt.%. These results indicate that the mechanical performance of the POC-PEG elastomers could be well adjusted by the PEG content. Because of the longer molecular chain of PEG compared with other small monomers, an increase in PEG content leads to decreased crosslinking density. On this basis, the mechanical strength and modulus of the elastomers decrease and the elongation at break increases with increasing PEG content.

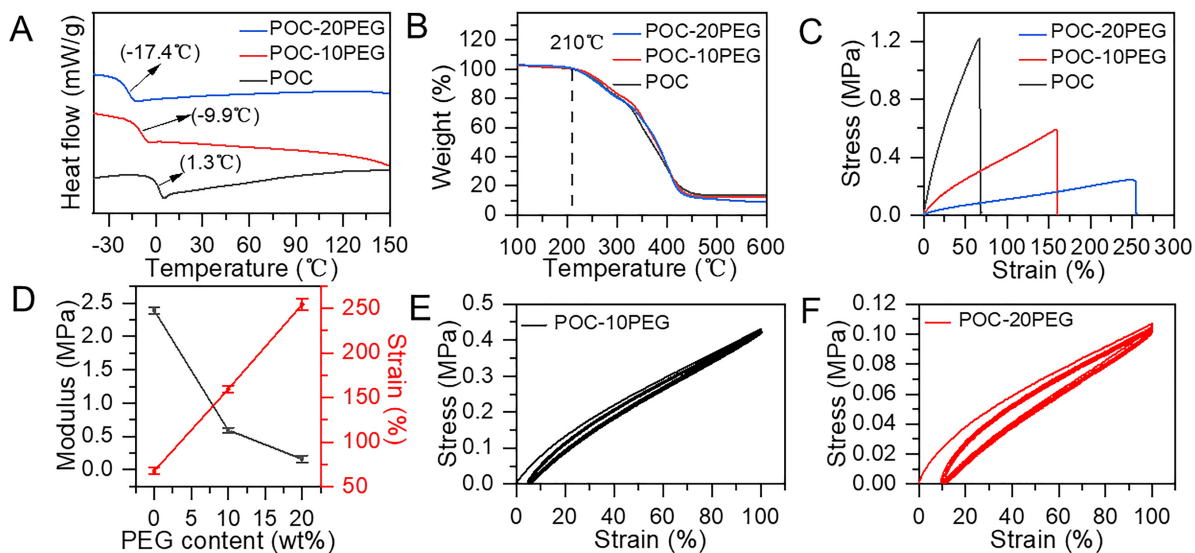


Figure 2. Thermodynamic and mechanical properties of POC-PEG elastomers. (A) DSC curves of POC, POC-10PEG and POC-20PEG elastomers. (B) TG curves. (C) stress-strain curves. (D) modulus and elongation at break of POC-PEG elastomers prepared for different contents of PEG. (E) tensile loading-unloading curves of POC-10PEG elastomer. (F) tensile loading-unloading curves of POC-20PEG elastomer.

Figure 2E and F show the cyclic load-unload curves of POC-10PEG and POC-20PEG, respectively. Hysteresis loops are observed for both POC-10PEG and POC-20PEG, and the residual strains in the first load-unload curve for POC-10PEG and POC-20PEG are 4.5% and 9.6%, respectively. In the subsequent cycles, the load-unload curves almost overlap and the residual strains remain unchanged with increasing load-unload cycles. The integrated mechanical properties endow POC-PEG polyester elastomers with potential soft materials for flexible devices.

The POC-PEG/AgNW CPEs were prepared by introducing a AgNW layer on the surface of POC-10PEG films, according to the procedures illustrated in Figure 3A. AgNW was first prepared according to a previously reported method^[35]. From the SEM and TEM images displayed in Figure 3B and C, the prepared AgNW has a wire shape and their diameter is ~50 nm. Figure 3D shows the UV-Vis spectrum of the AgNW dispersion. As seen, the absorption peak at 380 nm was observed, further indicating the successful preparation of AgNWs^[38]. The AgNW layer was introduced onto the surface of the POC-PEG elastomer film by a droplet coating procedure. The thickness of the coated AgNW layer was adjusted by the coating time. As displayed in Figure 3E-G, the thickness of the AgNW layer is in the range of 1.3-4.4 μm . From the surface morphology of the POC-PEG/AgNW CPEs displayed in Figure 3H-J, the AgNW randomly stack and interlace to form a continuous network.

Tensile strain sensitivity of POC-PEG/AgNW CPEs

The POC-PEG/AgNW CPEs inherit the mechanical flexibility of the POC-PEG elastomers and exhibit conductivity due to the AgNW layer. Upon deformation, the AgNW network changes accordingly and the POC-PEG/AgNW CPEs show excellent tensile strain sensitivity. The sensing mechanism of the POC-PEG/AgNW CPEs to applied strain is illustrated in Figure 4A. When gradually increasing strain is applied, the resistance of the PEG/AgNW CPEs increases accordingly [Figure 4B]. When the strain is kept at a certain value, the fluctuation of $\Delta R/R_0$ is small and step-like curves were recorded. From the linear fitting of the $\Delta R/R_0$ -strain curve, three gauge factors (GFs) were obtained, namely, 19.6, 82.5 and 231.6 in the

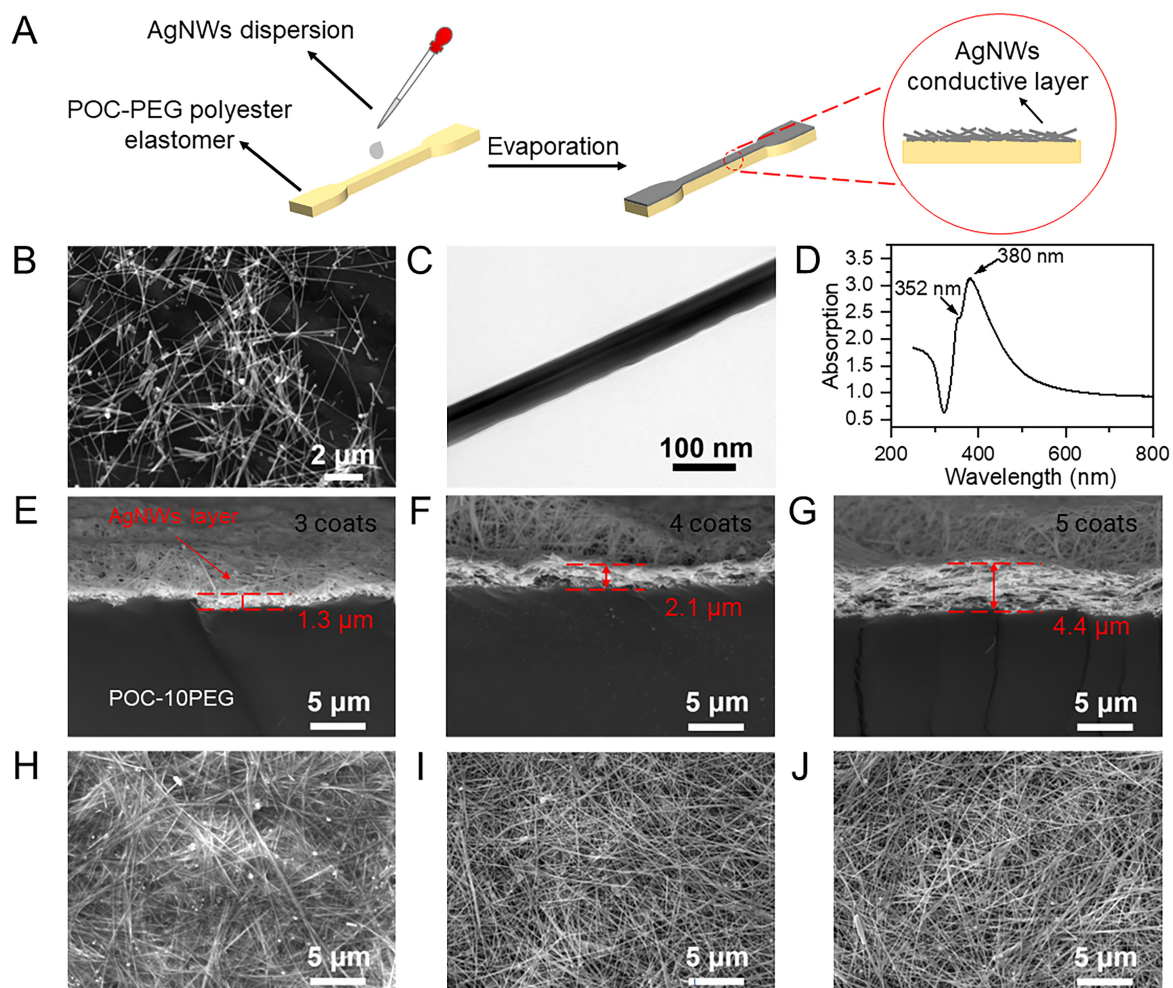


Figure 3. Preparation and characterization of POC-PEG/AgNW CPEs. (A) Illustration of preparation of POC-PEG/AgNW CPEs. (B) SEM image of AgNW. (C) TEM image of a single AgNW. (D) UV-Vis spectra of AgNW dispersed in ethanol (0.01 mg mL^{-1}). (E-G) SEM images of cross sections of POC-PEG/AgNW CPEs with different AgNW layer thicknesses. (H-J) SEM images of surface morphology of POC-PEG/AgNW CPEs with different AgNW layer thicknesses.

strain ranges of 0%-15%, 15%-40% and 40%-50%, respectively [Figure 4C]. Compared with other flexible sensors^[9,39-42], the POC-PEG/AgNW CPEs achieved a relatively high strain sensitivity.

There are three linear regions for the relative resistance change with increasing strain, which may be induced by the gradual destruction of the AgNW layer. When the AgNW layer is subjected to a tensile strain in the range of 0%-15% [Supplementary Figure 2], slippage between the AgNW occurs and the resistance slightly increases. With a further increase in strain, more and more cracks form because of the slippage between AgNW and the resistance changes obviously with increasing strain.

In addition, the POC-PEG/AgNW CPEs also respond reversibly to periodical strain for more than 800 cycles [Figure 4D]. From the insets of Figure 4E, the response is stable and the amplitude of $\Delta R/R_0$ is almost the same. The response time can be as low as 35 ms [Figure 4E], which ensures the fast detection of strain. Figure 4F shows the resistance response of a POC-PEG/AgNW CPE under different strains. As seen, the

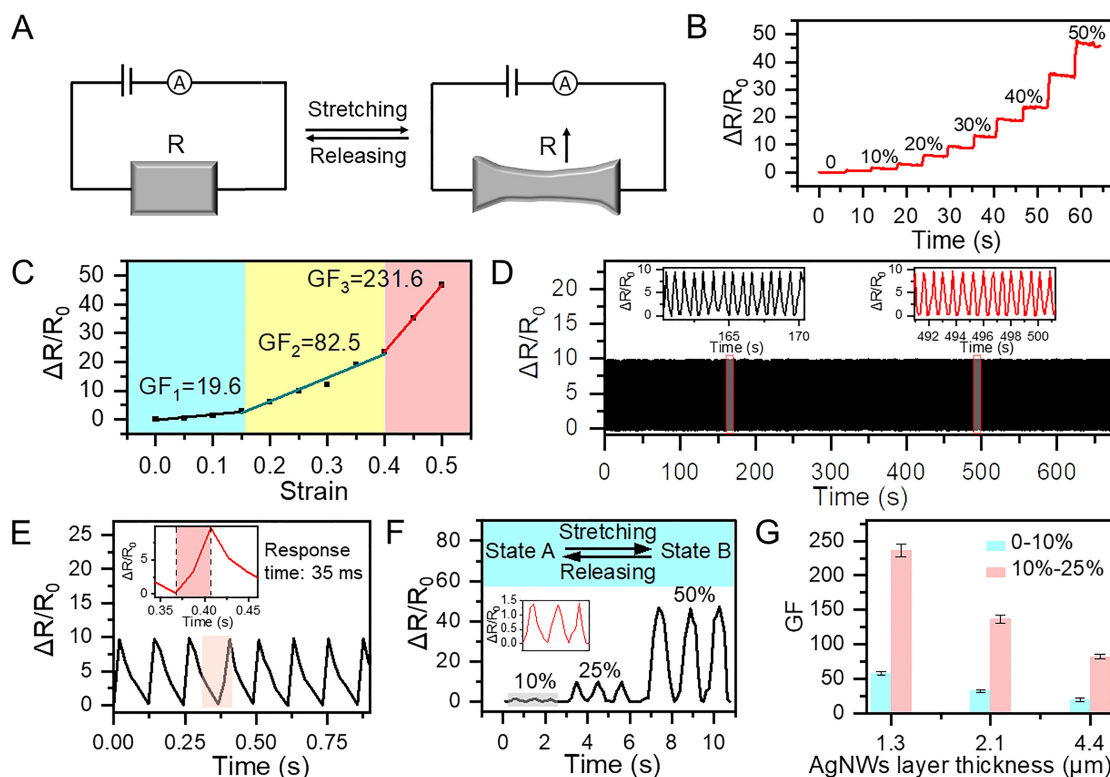


Figure 4. Tensile strain sensitivity of POC-PEG/AgNW CPEs. (A) Schematic illustration of strain sensing mechanism of POC-PEG/AgNW CPEs. (B) Resistance response of POC-PEG/AgNW CPEs to increasing strain from 0 to 50%. (C) Linear fitting of $\Delta R/R_0$ -strain curve. (D) Resistance response of POC-PEG/AgNW CPEs to cyclic strain of 25% over 800 cycles. (E) Response time of POC-PEG/AgNW CPEs to transient strain. (F) Resistance response of POC-PEG/AgNW CPEs to different strains of 10%, 25% and 50%. (G) Strain sensitivity of POC-PEG/AgNW CPEs containing AgNW layers with different thicknesses.

POC-PEG/AgNW CPE responds efficiently to cyclic strains of 10%, 25% and 50%.

Further investigations indicate that the tensile strain sensitivity of the POC-PEG/AgNW CPEs is dependent on the thickness of the AgNW layer [Figure 4G]. There is a general tendency that the GF decreases with increasing AgNW layer thickness. In the case of a AgNW layer thickness of 1.3 μm , the GF reaches 58.1 and 236.6 in the strain ranges of 0%-10% and 10%-25%, respectively. Under low strain loading, the conductive network is less affected by deformation, while under high strain loading, the conductive network undergoes a drastic variation and the GF is relatively high. In the case of a thin AgNW layer, the conductive network can easily change along with the POC-PEG elastomers and is sensitive to deformation. In contrast, for an elevated thickness, the robustness of the conductive network is enhanced and the sensitivity is lowered. This provides an opportunity to tune the strain sensitivity of the POC-PEG/AgNW CPEs by regulating the thickness of the AgNW layer.

Bending strain sensitivity of POC-PEG/AgNW CPEs

Similar to the resistance response of the POC-PEG/AgNW CPEs to tensile strain, bending strain also induces a variation in the AgNW conductive network that leads to resistance variation [Figure 5A]. With increasing bending strain, the resistance of the POC-PEG/AgNW CPEs increases gradually. When the bending strain is kept constant, $\Delta R/R_0$ maintains constant and a step-like response curve is recorded, indicating the stability of the POC-PEG/AgNW CPEs during the bending strain response [Figure 5B]. The GF is calculated according to $GF = (\Delta R/R_0)/\Delta\varepsilon$, where ε is calculated according to $\varepsilon = h/2r$ (h is the thickness

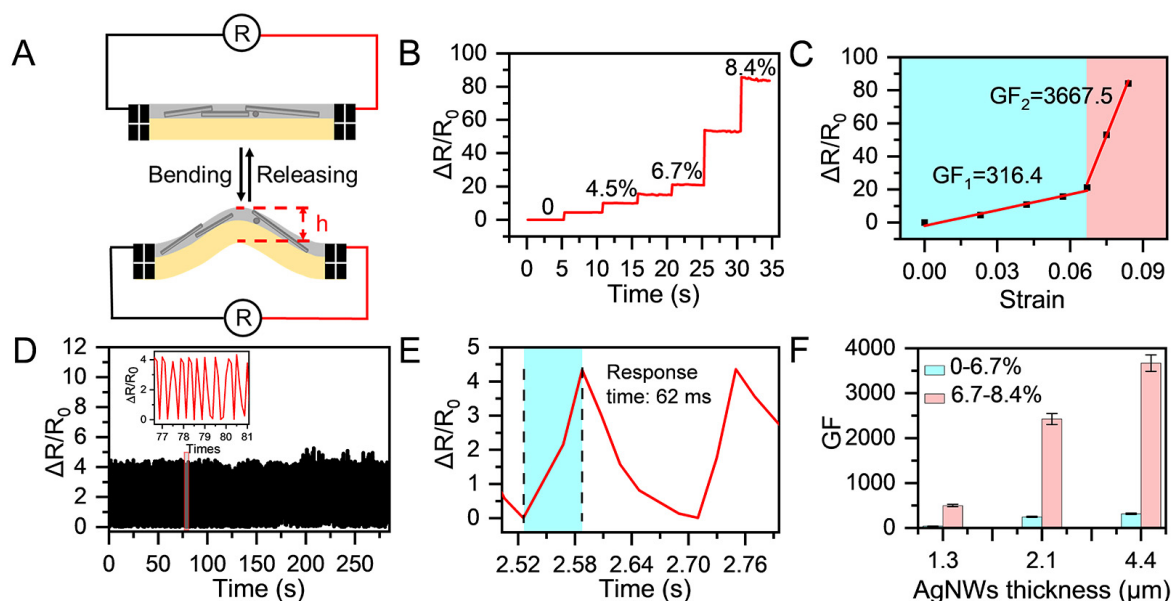


Figure 5. Bending strain sensitivity of POC-PEG/AgNW CPEs. (A) Schematic illustration of bending strain sensing mechanism of POC-PEG/AgNW CPEs. (B) Resistance response of POC-PEG/AgNW CPEs to increasing bending strain from 0-8.4%. (C) Linear fitting of $\Delta R/R_0$ -strain curve. (D) Resistance response of POC-PEG/AgNW CPEs to cyclic bending strain. (E) Response time of POC-PEG/AgNW CPEs to transient bending strain. (F) Strain sensitivity of POC-PEG/AgNW CPEs containing AgNW layers with different thicknesses.

of the material and r is the radius of curvature)^[43,44]. Figure 5C shows the linear fitting of the $\Delta R/R_0$ -strain curve, with two GFs obtained: $GF_1 = 316.4$ in the strain range of 0%-6.7%; $GF_2 = 3667.5$ in the strain range of 6.7%-8.4%. The POC-PEG/AgNW CPEs also efficiently respond to cyclic bending strain over 300 cycles [Figure 5D] in 62 ms [Figure 5E].

The strain sensitivity of the POC-PEG/AgNW CPEs is closely related to the thickness of the AgNW layer and sensing range [Figure 5F]. With fixed a AgNW layer thickness, the GF in the low bending strain range (0%-6.7%) is lower than that in the high bending strain range (6.7%-8.4%). In the case of a AgNW layer thickness of 1.3 μm , the GF reaches 42.6 and 499.4 in the strain ranges of 0%-6.7% and 6.7%-8.4%, respectively. Under a low bending strain loading, the AgNW conductive network is less affected and the GF is relatively low, while when a high bending strain is applied, the AgNW conductive network undergoes a drastic variation and the GF is high. When the AgNW layer thickness is increased, the GF decreases. The GF variation tendency with increasing AgNW layer thickness is opposite to that observed in the tensile strain response process. A possible reason for the decreasing GF with increasing AgNW layer thickness is as follows. When the thickness of the AgNW conductive layer is increased, a fluffy layer of AgNWs is obtained. Bending of the POC-PEG/AgNW CPEs induces full contact of the AgNWs and the high sensitivity of the CPEs to bending strain.

Wearable sensors based on POC-PEG/AgNW CPEs

On the basis of the high sensitivity of the POC-PEG/AgNW CPEs to tensile and bending strain, wearable and wireless strain sensors are further assembled by connecting flexible sensors to our previously established Bluetooth signal transmission system^[36,37]. Utilizing such sensors, various human motions and physiological activities were monitored. By mounting a sensor on a finger, joint bending was monitored by the resistance variation [Figure 6A and Supplementary Video 1]. Bending of the finger joint leads to an increase in resistance, while the resistance decreases when the finger joint is unbent. Different bending

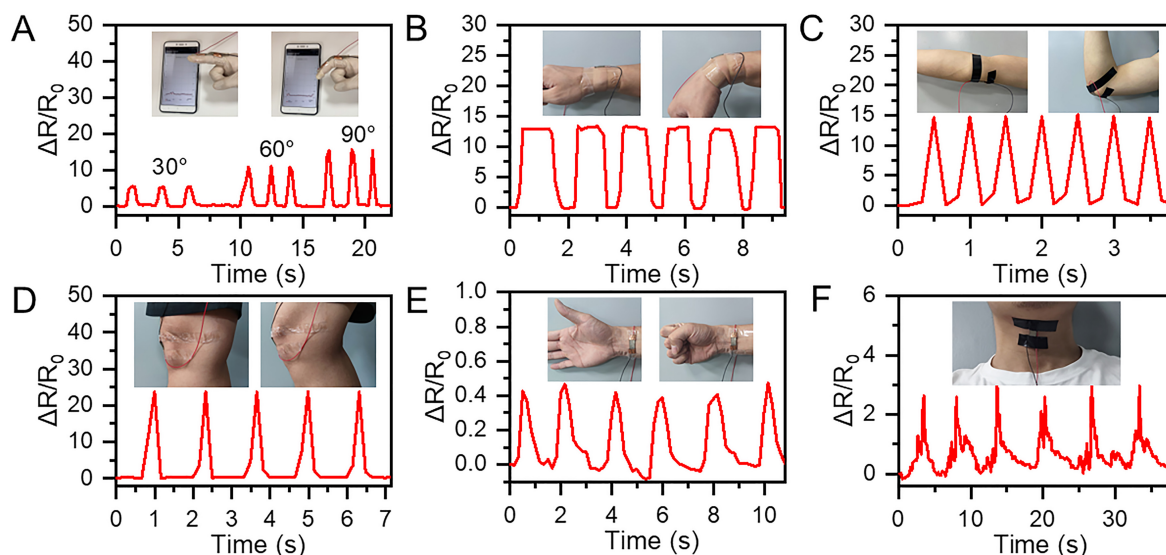


Figure 6. Wearable and wireless strain sensors of POC-PEG/AgNW CPEs for human motion monitoring. (A) Resistance response of sensor to joint bending. (B) Wrist bending. (C) Elbow bending. (D) Knee bending during walking. (E) Tendon motion caused by fist clenching. (F) The movement of prominentia laryngea induced by swallowing.

angles could be reflected by the amplitude of the resistance variation. In a similar manner, wrist, elbow and knee bending were also successfully detected [Figure 6B-D and Supplementary Video 2].

Due to the high strain sensitivity of the POC-PEG/AgNW CPEs, such sensors also have the ability to monitor small activities. Figure 6E shows the resistance response of the sensor to the tendon motion caused by fist clenching. As seen, periodical fist clenching induced an obvious resistance response and the tendon motion was monitored. Furthermore, by fixing a sensor near the prominentia laryngea, swallowing was also monitored by recording the resistance response induced by prominentia laryngeal motion [Figure 6F]. These results demonstrate that the POC-PEG/AgNW CPEs could be utilized in the construction of wearable and wireless sensors for both large strains induced by joint bending and small strains induced by physiological activities.

Degradability of POC-PEG/AgNW CPEs

The degradability of the POC-PEG/AgNW CPEs under different conditions was further evaluated. As shown in Figure 7A, the citric acid-based CPEs were degradable because of the cleavage of the ester bond in the polymer chain. Figure 7B and C display photographs of a POC-PEG/AgNW CPE soaked in a PBS buffer (pH 7.3) and a 0.1 mol L⁻¹ NaOH aqueous solution, respectively. As seen, the POC-PEG/AgNW CPE continuously swells for 0-2 months and then begins to gradually degrade in 2-5 months, exhibiting a slow degradation rate. In contrast, when the POC-PEG/AgNW CPE was soaked in a 0.1 mol L⁻¹ NaOH aqueous solution, the CPE sheet almost disappeared within only 6 h, indicating its degradation ability.

To gain insights into the degradation behavior, gel permeation chromatography curves of the polyester elastomer prepolymer and POC-PEG/AgNW CPE after being degraded in a 0.1 mol L⁻¹ NaOH aqueous solution for 10 d were collected. Figure 7D and E show the flow curve and molecular weight distribution curve of the prepolymer of the citric acid-based polyester elastomer, respectively. The weight average molecular weight (M_w) of the sample is $M_w = 4298 \text{ g mol}^{-1}$. For the sample after degradation, M_w for most of the polymers decreased to 467 g mol^{-1} [Figure 7F]. According to the molecular weight distribution curve in

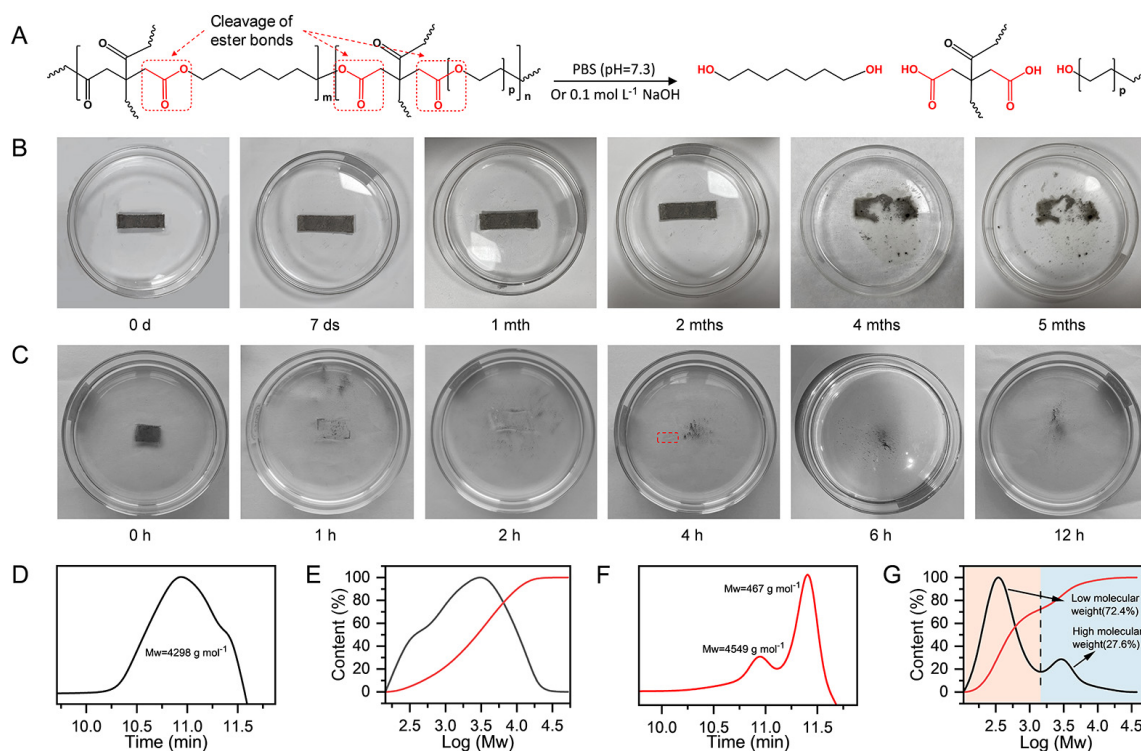


Figure 7. Degradability test of POC-PEG/AgNW CPEs. (A) Schematic diagram of hydrolytic degradation of citric acid-based CPEs. (B) Photographs of POC-PEG/AgNW CPE soaked in PBS buffer for 0-5 months. (C) Photographs of POC-PEG/AgNW CPE soaked in 0.1 mol L⁻¹ NaOH aqueous solution for 0-12 h. (D) Elution curves of prepolymers of POC-PEG polyester elastomer. (E) Molecular weight distribution curve of prepolymer of POC-PEG polyester elastomer. (F) Elution curve of POC-PEG/AgNW CPE after degradation in 0.1 mol L⁻¹ NaOH for 10 d. (G) Molecular weight distribution curve of POC-PEG/AgNW CPE after being soaked in 0.1 mol L⁻¹ NaOH for 10 d.

Figure 7G, the contents of the low and high molecular weight polymers are 72.4% and 27.6%, respectively. This means that most of the citric acid-based CPEs have been degraded via breakage of the polymer chain. This demonstrates that such POC-PEG/AgNW CPEs have the ability to degrade and could be used as key materials for green electronic devices.

CONCLUSIONS

In conclusion, degradable citric acid-based conductive polyester elastomers have been prepared by coating a silver nanowire layer on the surface of polyester elastomer films. The tensile strength, elongation at break and modulus of the polyester elastomers were found to be closely related to the feeding content of poly(ethylene glycol) during the melt polycondensation process. The excellent response ability of the conductive polyester elastomers to both tensile and bending strain and the strain sensitivity could be regulated by the thickness of the silver nanowire layer. On the basis of strain sensitivity, the conductive polyester elastomers were utilized as key sensitive materials for wearable and wireless sensors for the monitoring of various human motions and physiological activities. Degradability testing indicated that the conductive polyester elastomers have outstanding degradation ability in both neutral conditions and alkaline conditions. Overall, this work not only presents novel flexible electronic materials for further soft and wearable sensors but also provides an opportunity to develop sustainable electronics using degradable materials.

DECLARATIONS

Acknowledgments

The authors are thankful for the financial support from the National Natural Science Foundation of China (No. 51603164), the Natural Science Foundation of Shaanxi Province (No. 2019JM-124), the Natural Science Foundation of Shaanxi Provincial Department of Education (No. 20JS062), the Innovative Talents Promotion Plan-Young Science and Technology Star Project (No. 2021KJXX-42), and the Young Talent Fund of the University Association for Science and Technology in Shaanxi, China (No. 20170706).

Authors' contributions

Methodology, investigation, writing - original draft: Wang Z

Supervision, project administration: Zhou H

Writing - review & editing: Zhou H, Zhang H, Zhang G

Data curation, formal analysis: Zheng B

Methodology, investigation: Gao Y

Supervision, validation, methodology: Jin X, Ma A

Availability of data and materials

Not applicable.

Financial support and sponsorship

This work was supported by National Natural Science Foundation of China (No. 51603164), the Natural Science Foundation of Shaanxi Province (No. 2019JM-124), the Natural Science Foundation of Shaanxi Provincial Department of Education (No. 20JS062), the Innovative Talents Promotion Plan-Young Science and Technology Star Project (No. 2021KJXX-42), Outstanding Young Talents in Colleges and Universities of Shaanxi Province and the Young Talent Fund of the University Association for Science and Technology in Shaanxi, China (No. 20170706).

Conflicts of interest

All authors declared that there are no conflicts of interest.

Ethical approval and consent to participate

All procedures performed in this study involved non-invasive placement of the device on the skin and posed no risk to participants. Therefore, the study qualified for exemption from ethical review. Informed consent was obtained from all participants prior to their involvement.

Consent for publication

Not applicable.

Copyright

© The Author(s) 2022.

REFERENCES

1. Patel S, Ershad F, Zhao M, et al. Wearable electronics for skin wound monitoring and healing. *Soft Sci* 2022;2:9. DOI
2. Chen J, Zhu Y, Chang X, et al. Recent progress in essential functions of soft electronic skin. *Adv Funct Mater* 2021;31:2104686. DOI
3. Zhu J, Zhou C, Zhang M. Recent progress in flexible tactile sensor systems: from design to application. *Soft Sci* 2021;1:3. DOI
4. Vallem V, Sargolzaeiaval Y, Ozturk M, Lai YC, Dickey MD. Energy harvesting and storage with soft and stretchable materials. *Adv Mater* 2021;33:e2004832. DOI PubMed
5. Yu J, Zhang K, Deng Y. Recent progress in pressure and temperature tactile sensors: principle, classification, integration and outlook. *Soft Sci* 2021;1:6. DOI
6. Gui Q, He Y, Wang Y. Soft electronics based on liquid conductors. *Adv Electron Mater* 2021;7:2000780. DOI
7. Wolf MP, Salieb-beugelaar GB, Hunziker P. PDMS with designer functionalities-properties, modifications strategies, and applications. *Progr Polym Sci* 2018;83:97-134. DOI

8. Qi D, Zhang K, Tian G, Jiang B, Huang Y. Stretchable electronics based on PDMS substrates. *Adv Mater* 2021;33:e2003155. DOI PubMed
9. Zhang K, Shi X, Chen J, Xiong T, Jiang B, Huang Y. Self-healing and stretchable PDMS-based bifunctional sensor enabled by synergistic dynamic interactions. *Chem Eng J* 2021;412:128734. DOI
10. Yang Y, Cao Z, He P, Shi L, Sun J. Ti3C2Tx MXene-graphene composite films for wearable strain sensors featured with high sensitivity and large range of linear response. *Nano Energy* 2019;66:104134. DOI
11. Cai Y, Zhang X, Wang G, et al. A flexible ultra-sensitive triboelectric tactile sensor of wrinkled PDMS/MXene composite films for E-skin. *Nano Energy* 2021;81:105663. DOI
12. Wei Q, Chen G, Pan H, et al. MXene-sponge based high-performance piezoresistive sensor for wearable biomonitoring and real-time tactile sensing. *Small Methods* 2022;6:e2101051. DOI PubMed
13. Zhou Y, Zhan P, Ren M, et al. Significant stretchability enhancement of a crack-based strain sensor combined with high sensitivity and superior durability for motion monitoring. *ACS Appl Mater Interfaces* 2019;11:7405-14. DOI PubMed
14. Zhang Y, Zhu X, Liu Y, et al. Ultra-stretchable monofilament flexible sensor with low hysteresis and linearity based on MWCNTs/Ecoflex composite materials. *Macro Mater Eng* 2021;306:2100113. DOI
15. Yue X, Yang J, Gao J, et al. Wearable hydroxylated MWCNTs/ecoflex composite strain sensor with high comprehensive performance based on electron irradiation. *Compos Sci Technol* 2022;226:109537. DOI
16. Wang Y, Yokota T, Someya T. Electrospun nanofiber-based soft electronics. *NPG Asia Mater* 2021;13:22. DOI
17. Cho KW, Sunwoo SH, Hong YJ, et al. Soft bioelectronics based on nanomaterials. *Chem Rev* 2022;122:5068-143. DOI PubMed
18. Lyu Q, Gong S, Yin J, Dyson JM, Cheng W. Soft wearable healthcare materials and devices. *Adv Healthc Mater* 2021;10:e2100577. DOI PubMed
19. Kim MG, Brown DK, Brand O. Nanofabrication for all-soft and high-density electronic devices based on liquid metal. *Nat Commun* 2020;11:1002. DOI PubMed PMC
20. Peng S, Yu Y, Wu S, Wang CH. Conductive polymer nanocomposites for stretchable electronics: material selection, design, and applications. *ACS Appl Mater Interfaces* 2021;13:43831-54. DOI PubMed
21. McLellan K, Yoon Y, Leung SN, Ko SH. Recent progress in transparent conductors based on nanomaterials: advancements and challenges. *Adv Mater Technol* 2020;5:1900939. DOI
22. Wang C, Wang C, Huang Z, Xu S. Materials and structures toward soft electronics. *Adv Mater* 2018;30:e1801368. DOI PubMed
23. Chiong JA, Tran H, Lin Y, Zheng Y, Bao Z. Integrating emerging polymer chemistries for the advancement of recyclable, biodegradable, and biocompatible electronics. *Adv Sci (Weinh)* 2021;8:e2101233. DOI PubMed PMC
24. Zhang Q, Song M, Xu Y, Wang W, Wang Z, Zhang L. Bio-based polyesters: recent progress and future prospects. *Progress in Polymer Science* 2021;120:101430. DOI
25. Davenport Huyer L, Bannerman AD, Wang Y, et al. One-pot synthesis of unsaturated polyester bioelastomer with controllable material curing for microscale designs. *Adv Healthc Mater* 2019;8:e1900245. DOI PubMed
26. Chen CJ, Huang BW, Tseng PJ, et al. Low-mass liquid crystalline materials blended in recycled thermoplastic polyester elastomer for corrosion inhibitor application. *Polymers (Basel)* 2021;13:3188. DOI PubMed PMC
27. Satti SM, Shah AA. Polyester-based biodegradable plastics: an approach towards sustainable development. *Lett Appl Microbiol* 2020;70:413-30. DOI PubMed
28. Tang S, Li J, Wang R, et al. Current trends in bio-based elastomer materials. *SusMat* 2022;2:2-33. DOI
29. Siehr A, Flory C, Callaway T, Schumacher RJ, Siegel RA, Shen W. Implantable and degradable thermoplastic elastomer. *ACS Biomater Sci Eng* 2021;7:5598-610. DOI PubMed
30. De Hoe GX, Zumstein MT, Tiegs BJ, et al. Sustainable polyester elastomers from lactones: synthesis, properties, and enzymatic hydrolyzability. *J Am Chem Soc* 2018;140:963-73. DOI PubMed
31. Wang D, Tang Z, Wang Z, Zhang L, Guo B. A bio-based, robust and recyclable thermoset polyester elastomer by using an inverse vulcanised polysulfide as a crosslinker. *Polym Chem* 2022;13:485-91. DOI
32. Wei T, Lei L, Kang H, et al. Tough Bio-based elastomer nanocomposites with high performance for engineering applications. *Adv Eng Mater* 2012;14:112-8. DOI
33. Kang H, Li X, Xue J, et al. Preparation and characterization of high strength and noncytotoxic bioelastomers containing isosorbide. *RSC Adv* 2014;4:19462. DOI
34. Gao Y, Xue J, Zhang L, Wang Z. Synthesis of bio-based polyester elastomers and evaluation of their in vivo biocompatibility and biodegradability as biomedical materials. *Biomater Sci* 2022;10:3924-34. DOI PubMed
35. Li B, Ye S, Stewart IE, Alvarez S, Wiley BJ. Synthesis and purification of silver nanowires to make conducting films with a transmittance of 99%. *Nano Lett* 2015;15:6722-6. DOI PubMed
36. Zhou H, Lai J, Jin X, et al. Intrinsically adhesive, highly sensitive and temperature tolerant flexible sensors based on double network organohydrogels. *Chem Eng J* 2021;413:127544. DOI
37. Zhou H, Lai J, Zheng B, et al. From glutinous-rice-inspired adhesive organohydrogels to flexible electronic devices toward wearable sensing, power supply, and energy storage. *Adv Funct Materials* 2022;32:2108423. DOI
38. Chang MH, Cho HA, Kim YS, Lee EJ, Kim JY. Thin and long silver nanowires self-assembled in ionic liquids as a soft template: electrical and optical properties. *Nanoscale Res Lett* 2014;9:330. DOI PubMed PMC
39. Peng Y, Zhao L, Yang C, et al. Super tough and strong self-healing elastomers based on polyampholytes. *J Mater Chem A*

- 2018;6:19066-74. [DOI](#)
40. Yiming B, Han Y, Han Z, et al. A mechanically robust and versatile liquid-free ionic conductive elastomer. *Adv Mater* 2021;33:e2006111. [DOI](#) [PubMed](#)
 41. Lu C, Wang C, Wang J, Yong Q, Chu F. Integration of hydrogen bonding interaction and Schiff-base chemistry toward self-healing, anti-freezing, and conductive elastomer. *Chem Eng J* 2021;425:130652. [DOI](#)
 42. Wang M, Lai Z, Jin X, Sun T, Liu H, Qi H. Multifunctional liquid-free ionic conductive elastomer fabricated by liquid metal induced polymerization. *Adv Funct Mater* 2021;31:2101957. [DOI](#)
 43. Sun H, Dai K, Zhai W, et al. A highly sensitive and stretchable yarn strain sensor for human motion tracking utilizing a wrinkle-assisted crack structure. *ACS Appl Mater Interfaces* 2019;11:36052-62. [DOI](#) [PubMed](#)
 44. Liu H, Jiang H, Du F, Zhang D, Li Z, Zhou H. Flexible and degradable paper-based strain sensor with low cost. *ACS Sustain Chem Eng* 2017;5:10538-43. [DOI](#)